HYDROGEN STUDIES INCLUDING SIMULATIONS FOR THREE BODY ASSOCIATION AND DEVELOPMENT OF IN-SITU SILICON PASSIVATION

A Thesis
Presented to
The Academic Faculty

by

Tharon D. Morrison

In Partial Fulfillment of
the Requirements for the Dean's Scholars Honors Program and
the Degree of Bachelor's of Science in Physics Honors in the
Physics Department

University of Texas at Austin

HYDROGEN STUDIES INCLUDING SIMULATIONS FOR THREE BODY ASSOCIATION AND DEVELOPMENT OF IN-SITU SILICON PASSIVATION

Approved by:

Professor Mark G. Raizen, Advisor
Center for Nonlinear Dynamics and the
Physics Department
University of Texas at Austin

Date Approved: _____

DEAN'S SCHOLARS PERMISSIONS

I grant the Deans Scholars Program permission to post a copy of my thesis on the University of Texas Digital Repository. For more information, visit http://repositories.lib.utexas.edu/about.

Hydrogen Studies Including Simulations for Three Body Association and Development of In-Situ Silicon Passivation

Tharon D. Morrison _____ Date _____

Mark G. Raizen _____ Date _____

To my parents, without them I could not be who I am today.

"I ask you to look both ways. For the road to a knowledge of the stars leads through the atom; and important knowledge of the atom has been reached through the stars."

– Sir Arthur Eddington (1882 - 1944), Stars and Atoms (1928), Lecture 1

ACKNOWLEDGEMENTS

First and foremost, I would like to thank my advisor Mark Raizen. Mark took me on when I was just starting off at the University of Texas at Austin. Since then I have learned multitudes about running experiments, managing a laboratory, and being a physicist in general through his help and example.

Many graduate students have helped me along the way in the Raizen Lab. Tom Mazur always gave me great advice about what I could use in an experiment to make it better. Isaac Chavez helped me see potential problems in my designs so that I could prevent them before they became an issue. Kevin Melin for all of his help addressing anything I needed in terms of computers. Jamie Garnder for helping introduce me to the lab and teaching the ins and outs. Karl Burkhardt for his sympathy, help in troubleshooting an experiment, and chemistry prowess. Alina Blinova for all of the discussions. Georgios Stratis, Erik Anciaux, Jianyong Mo, and Akarsh Simha for being there for me in general. And the entire Raizen Lab because they are an extraordinary group of people.

I would also like to thank Rodrigo Castillo-Garza. Rodrigo would always provide a new frame of looking at things that always would add to my perspective.

I would also like to thank Evan Ott. He has been my roommate the entire time I have been at the University of Texas and has been a quintessential part of me grappling with many of the obstacles that I have had to leap over these past years.

And lastly, I would like to thank my parents. They have always been so very supportive of me. I do not know what I would have done without them.

TABLE OF CONTENTS

LIST OF TABLES

LIST OF FIGURES

SUMMARY

Hydrogen, for many years, has been a gateway for understanding physics in all measures and strides. This paper adds to this vibrant tradition of hydrogen, first with a computational analysis of a proposed experiment to investigate the formation via three body association of the first molecules of the universe, diatomic hydrogen and secondly with development of a technique to terminate the surface of a silicon crystal with hydrogen isotopes to eventually make measurements of the neutrino mass.

In order for the three body association of hydrogen to occur, particular temperature and density constraints must be met. These have been fleshed out in the following pages. A computational simulation of a hexapole lens acting on the hydrogen atoms suggests that it would be possible to create an experiment to make the first ever measurements of the spin-depolarized chemical process that created the first molecules. The simulation shows that using a Gaussian cube of 10^6 hydrogen atoms at a temperature of 10^{-9}K and a hexapole lens capable of creating a field gradient of 10^6 Tesla per square meter, a density of 10^{21} atoms per cubic meter would be achieved. Then with a laser probing for hydrogen molecules, the first spin-depolarized measurements of three body association of hydrogen could be made.

This work also reviews a technique in the final stages of development for tritium passivated silicon in vacuum. There are many advantages to using tritium passivated silicon as a source for beta decay electrons. The passivation quality from the developing technique can be addressed using elastic scattering of helium off of the passivated surface.

CHAPTER I

INTRODUCTION TO THREE BODY ASSOCIATION

The formation of hydrogen molecules sets the time scale for the universe. In a two-body scenario the bonding cross section is significantly smaller than what would promote primordial star formation at the observed rate [1]. Hence astronomers and physicists alike have moved forward with the idea that this reaction would be catalyzed by a third body, primarily another hydrogen atom.

1.1 Implications of Formation Rate

The rate of formation of molecular hydrogen governs the collapse and cooling of the early universe gases into Population III protostars [2]. Population III stars resulting from these protostars are theorized to have been the first stars in the universe formed solely out of the gravitational collapse of hydrogen atoms [3]. Unfortunately these stars would have finished their life cycles early in the history of our universe so that observations of limited quality can actually be made from observational astronomy.

1.2 Discussion of Possible Reactions

From classical mechanics, two attracted bodies will tend to form stable orbits or scatter off one another. Therefore, energy must be transported out of the two hydrogen atoms in order for them to bond as hydrogen molecules. A scattering event is very likely between two hydrogen atoms; therefore, it is often thought that a third body would catalyze the reaction by carrying out with it some of the excess energy. Previous theories used an electron and photon to mediate this energy flow. This would have been mediated by the reaction:

$$H + e^- \rightarrow H^- + \gamma \tag{1}$$

$$H^- + H \rightarrow H_2 + e^- \tag{2}$$

An experimental measurement of this type of molecular hydrogen formation was conducted [4]. While this particular type reaction contributed to the formation of early hydrogen molecules, it is unlikely, as pointed out by Turk *et al.* [2], that this would be the dominant factor in early molecular formation due to its dependence on electron concentration. Therefore neutral three body association is thought to be predominant in the formation of molecular hydrogen [5]. These neutral three body association reactions include:

$$H + H + H \rightarrow H_2 + H \tag{3}$$

$$H + H + H_2 \rightarrow H_2 + H_2 \tag{4}$$

$$D + D + D \rightarrow D_2 + D \tag{5}$$

$$D + D + D_2 \rightarrow D_2 + D_2 \tag{6}$$

Although theoretical calculations have been made on these classes of reactions [6], there has been no way to experimentally measure these reaction rates for spin depolarized atoms. The spin polarized case has been measured [7]. This however is not representative of hydrogen in the early universe. The dissociation of hydrogen molecules has also been studied intensively [8].

1.3 Motivation for Three Body Association Experiment

Obviously, there exist many constraints on an experiment attempting to measure neutral three body association in the spin depolarized case. The biggest constraint is the density of the hydrogen atoms due to the dependence of concentration of most reaction rates. In terms of signal results, this is around 10^{15} atoms/cc (10^{21} atoms/m^3)[9]. Therefore, if the target density is achieved, a reasonable signal to noise ratio will be possible. Another constraint on these measurements relevant to Population III protostars is the temperature. A temperature range of 200 to 2000 K during the collapse will be useful for comparison to the early universe [10].

These are the constraints with which to gauge the feasibility of an experiment. In the next section, a more detailed description follows for a simulation to judge a proposed experiment's likelihood to meet these conditions.

CHAPTER II

METHODOLOGY FOR THREE BODY ASSOCIATION PARAMETER SIMULATION

Subject to the constraints in the previous chapter, a proposed experiment to measure the formation rate of molecular hydrogen is evaluated.

2.1 The Proposed Experiment

The following experiment was proposed by Mark Raizen and initially discussed by Daniel Raimi-Zlatic [9].

The entirety of the experiment hinges on using magnetic forces to accelerate atomic hydrogen into a focal point. The force ($\vec{F}$) on a magnetic species of hydrogen goes as:

$$\vec{F} = -\vec{\nabla}U = -\vec{\nabla}(-\vec{\mu}\cdot\vec{B}) \tag{7}$$

where U is the potential, $\vec{\mu}$ is the magnetic moment of the hydrogen atom, and $\vec{B}$ is the magnetic field. The experiment will use a magnetic field of a pulsed hexapole lens [11]. The magnetic field of a hexapole lens goes as:

$$B = \frac{1}{2}B_0 r^2 \tag{8}$$

where B_0 is a constant of the magnetic field gradient, and r is the radial distance from the center axis of the hexapole lens. $\vec{\mu}$ is given by:

$$\vec{\mu} = m_f g \mu_b \hat{\mu} \tag{9}$$

where m_f is the magnetic quantum number of the hydrogen, g is the g-factor corresponding to hydrogen, μ_b is the Bohr Magneton, and $\hat{\mu}$ is the unit vector pointing in the direction of the magnetic moment [12]. The direction on $\hat{\mu}$ is selected to be

either with or against the gradient of the magnetic field similarly to the Stern-Gerlach Experiment. For this simulation both m_f and g are set to 1 and the alignment of $\hat{\mu}$ to the magnetic field gradient is such that the force will be towards the center axis of the hexapole lens. By a few vector identities these relationships simplify Equation 7 to:

$$\vec{F} = -m_f g \mu_b B_0 r \hat{r} \tag{10}$$

where r is the distance from the center of the hexapole lens. Then a coordinate change for $r^2 = x^2 + y^2$ will leave a set of equations in the typical Cartesian coordinates. This leaves us with the following differential equations when assuming separable solutions and taking the classical assumption of $\vec{F} = m_H \vec{a}$, with m_H being the mass of the hydrogen atom and $\vec{a}$ being the acceleration:

$$\frac{d^2x}{dt^2} = -\frac{m_f g \mu_b B_0}{m_H} x \tag{11}$$

$$\frac{d^2y}{dt^2} = -\frac{m_f g \mu_b B_0}{m_H} y \tag{12}$$

$$\frac{d^2z}{dt^2} = 0. \tag{13}$$

With these differential equations, a cluster of perfectly cold atoms would be focused to the center of the hexapole lens at a time equal to one quarter of the period of oscillation (P) for the harmonic potential. In other words $t = \frac{1}{4}P = \frac{1}{4}\frac{2\pi}{\omega}$ with ω being the angular frequency of the harmonic potential where:

$$\omega = \sqrt{\frac{m_f g \mu_b B_0}{m_H}}. \tag{14}$$

However, this is non-ideal as it would leave the hydrogen spin polarized.

2.2 Evaluation of Parameters

Based on Equations 11, 12, and 13 for when the magnetic field is on, and assuming a typical $\vec{r} = \vec{r_0} + \vec{v}t$ solution when the magnetic field is off, the ability of this set-up

to address three body association can be evaluated.

Given that the magnetic field is on for a time t_d, the final position of the particle after t_d is given by the following equations:

$$x(t_d) = x_0 \cos(\omega t_d) + \frac{v_{0x}}{\omega} \sin(\omega t_d) \tag{15}$$

$$y(t_d) = y_0 \cos(\omega t_d) + \frac{v_{0y}}{\omega} \sin(\omega t_d) \tag{16}$$

$$z(t_d) = z_0 + v_{0z} t_d. \tag{17}$$

Initial positions are found by sampling from a Gaussian Distribution with a standard deviation decided by $2\sigma = L$ for box side lengths L_i. Initial velocities are found by sampling from the Maxwell-Boltzmann Distribution for a decided starting temperature[13].

2.2.1 Temperature

By taking the derivatives of Equations 15, 16, 17, the velocities of particles can be found. With the velocities, the kinetic energy of particles is used to evaluate the temperature (T), with k_b as the Boltzmann constant, and n particles with kinetic energy K_i:

$$T = \frac{2}{3k_b n} \Sigma_i^n K_i. \tag{18}$$

2.2.2 Density

The density is a little more challenging to compute than the temperature. The canonical solution for the density comes from Density Functional Theory [14]. From this, the Weighted Density Approximation is useful. The Weighted Density Approximation is:

$$\bar{\rho}(\vec{r}) = \int d\vec{r'} \rho(\vec{r} + \vec{r'}) w(r'). \tag{19}$$

The zeroth order of the weight function (w) is as follows[14]:

$$w(r') = \frac{3}{4\pi r'^3} = \frac{1}{V_i} \tag{20}$$

or V^{-1} of the volume V corresponding to a hydrogen atom on the wall of a sphere a distance r away. Because the positions of the particles are known in the simulation, the density $\rho(\vec{r} + \vec{r'})$ is simply:

$$\rho(\vec{r} + \vec{r'}) = \Sigma_i^n \delta(\vec{r_i}). \tag{21}$$

This simplifies the integral in Equation 19 to a summation:

$$\bar{\rho}(\vec{r}) = \Sigma_i^n \frac{3}{4\pi|\vec{r} - \vec{r_i}|^3}. \tag{22}$$

Therefore, the effective density of each hydrogen atom can be addressed. In terms of run-time for n hydrogen atoms, the hydrogen atom density runs as n^2 because of the comparison of two of the atoms positions. Each time-step requires reassessment of the density, therefore adding n^2 calculations with each time-step. Therefore, a mathematical prediction of when the cloud will collapse is useful in cutting down the number of time-steps (s) necessary to find the peak density. The derivation of the time to collapse ($t_{collapse}$) is done in Appendix A. The summary of this is:

$$t_{collapse} = \frac{\cot(\omega t_d)}{\omega}. \tag{23}$$

Now all of the machinery has been laid out to adequately address what limits the experiment. Not only can the peak temperature and density be addressed, but the instantaneous temperature and density can be used to even find a predicted percentage conversion rate in future simulations using theoretically predicted values of the reaction rate[5].

CHAPTER III

RESULTS FOR THREE BODY ASSOCIATION PARAMETER SIMULATION

Many iterations of the simulation were run with a variety of parameters. Magnetic fields gradients (B_0) from 10^4 to 10^8 T/m^2, numbers of particles (n) from 10^4 to 10^7 atoms, and a variety of drive times were tested. Drive times, however, are not entirely independent. To prevent cycling of the atoms in the harmonic potential of the pulsed magnetic field, the atoms need to be driven for a time (t_d):

$$t_d = a\frac{2\pi}{\omega} \tag{24}$$

where a is a number between 0 and 0.25. At 0.25, the particles should, on average, be at the center of the potential.

3.1 Temperature

In terms of meeting the temperature range relevant to Population III protostars, a magnetic field gradient of 10^6 T/m^2 and an a value of 0.125 achieve a temperature of 11 K given a Gaussian box of 0.01 m as a starting configuration. This temperature can be increased through an increase in the magnetic field gradient or an increase in the starting distance from the center axis of the potential. This spatial dependence of the final temperature dependence is discussed in Appendix C. Therefore, it is possible to achieve temperatures relevant for Population III protostars. A more thorough probe of the hydrogen formation rate as a function of temperature can be achieved by different starting configurations and magnetic field gradients. This ability to tune parameters may also be useful in the field of cold chemistry. However, it is a digression from this work's goals.

3.2 Density

In terms of the density, there are many viable parameters used to scan the effect of density. The two that are going to be focused on are *Configuration 1* and *Configuration 2*, summarized in Table 1. *Configuration 1* is a hypothetical example to prove the versatility of the method and is the same as that which was used in Section 3.1. The particles are driven for about 20.9 μs and the particles collapse about 0.211 μs later. *Configuration 2* is a physically relevant example because it drives the particles for 10 μs and allowing the cloud to collapse for 177 μs. This allows for a longer time to probe the evolution of the cloud while collapsing as well as a factor of 1000 in the time for hydrogen atoms to spin-depolarize. The configuration is nearly that of cooled hydrogen in an optical tweezer. Admittedly, the temperature achieved by this scheme is much less, nearly 2.8 mK. However, this can be adjusted using multiple initial tweezer configurations 1 cm above or below the z-axis to emulate the temperature effects of *Configuration 1*.

Table 1: Configuration Summary

Parameter Description		Configuration	
Set Parameters		1	2
n	Particles (atoms)	10^6	10^6
B_0	Magnetic Field Gradient (T/m^2)	10^6	10^5
T_0	Initial Temperature (K)	10^{-9}	10^{-10}
a	Drive Parameter (unitless)	0.125	0.03746
L_x	X Length of Gaussian Box (m)	0.01	0.003
L_y	Y Length of Gaussian Box (m)	0.01	10^{-5}
L_z	Z Length of Gaussian Box (m)	0.01	10^{-5}
Resultant Parameters		1	2
t_d	Drive Time (μs)	20.89	9.999
$t_{collapse}$	Time to Collapse (μs)	0.211	177.12
ρ_{peak}	Peak Density (atoms/m^3)	10^{22}	10^{24}
T_f	Final Temperature (K)	11.18	0.00275

3.2.1 Configuration 1

As seen in Figures 1 - 6 the average particle achieves a density of 10^{22} atoms/m^3. Therefore, this will work to get the particles into the critical density and temperature regime necessary for Population III protostars.

3.2.2 Configuration 2

As seen in Figures 7 - 12 the average particle achieves a density of 10^{24} atoms/m^3. Therefore, this will also achieve the necessary density in a physically relevant configuration.

3.3 Conclusion

Based on the simulation of hydrogen atoms in a pulsed harmonic potential like that of a hexapole lens, it is reasonable to suggest that this experiment could be done as a table top experiment to investigate the reaction rate of spin-depolarized formation of hydrogen molecules.

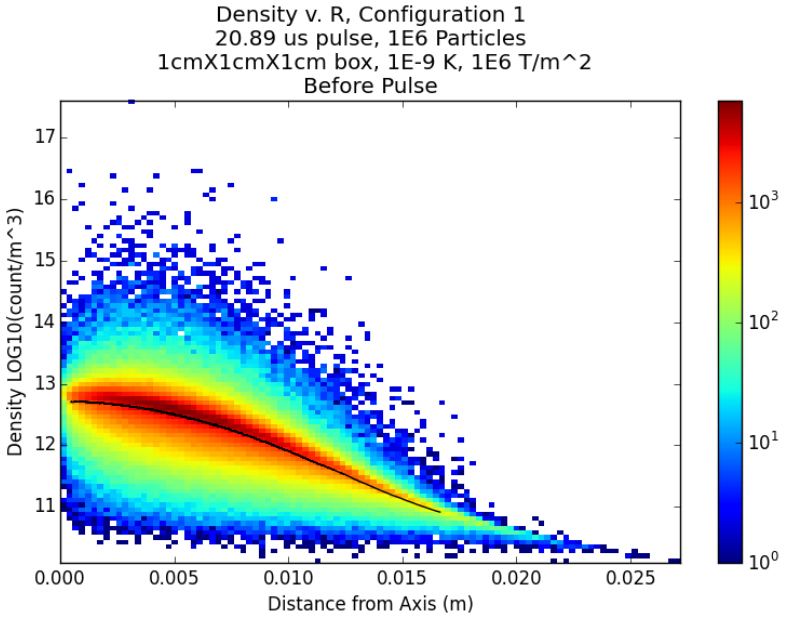

Figure 1: Configuration 1 - Initial Density vs. R. The average particle at R is in black. Color indicates number of particles.

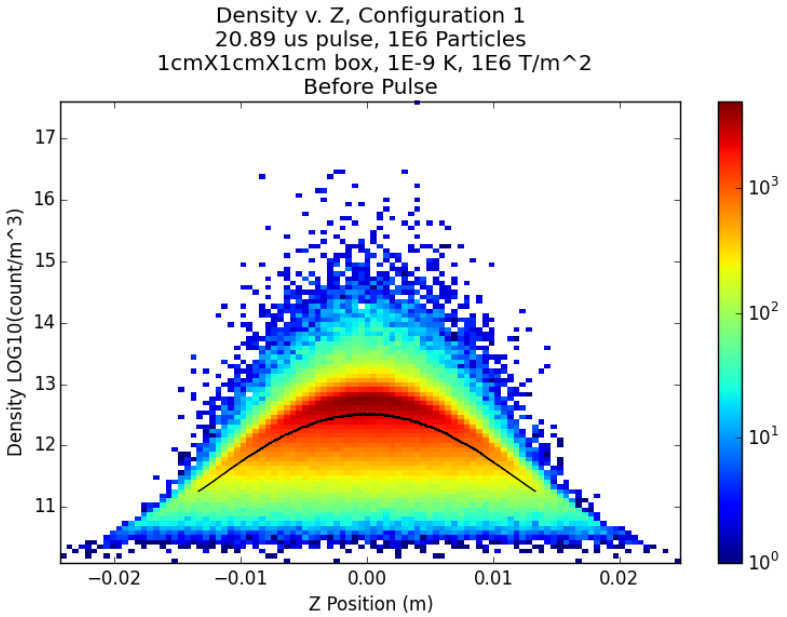

Figure 2: Configuration 1 - Initial Density vs. Z. The average particle at Z is in black. Color indicates number of particles.

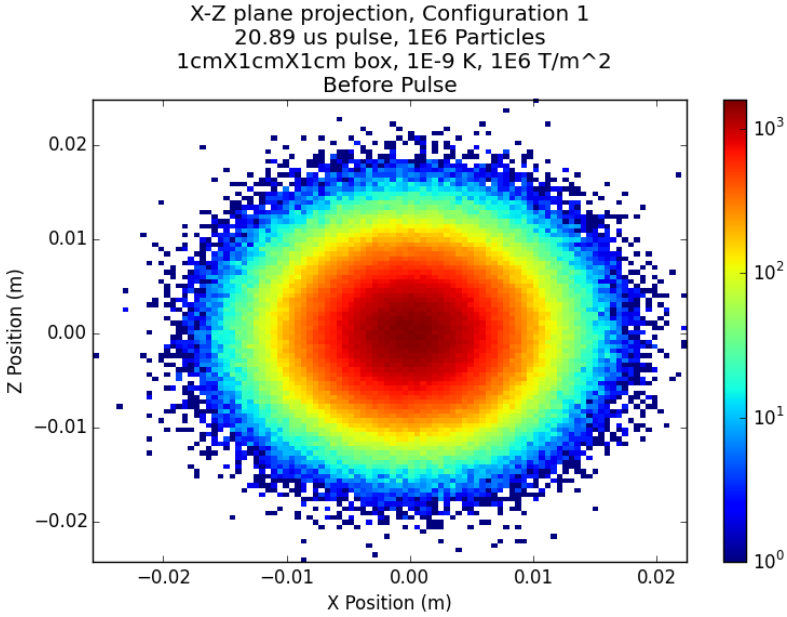

Figure 3: Configuration 1 - Initial X-Z projection of particles. Color indicates number of particles.

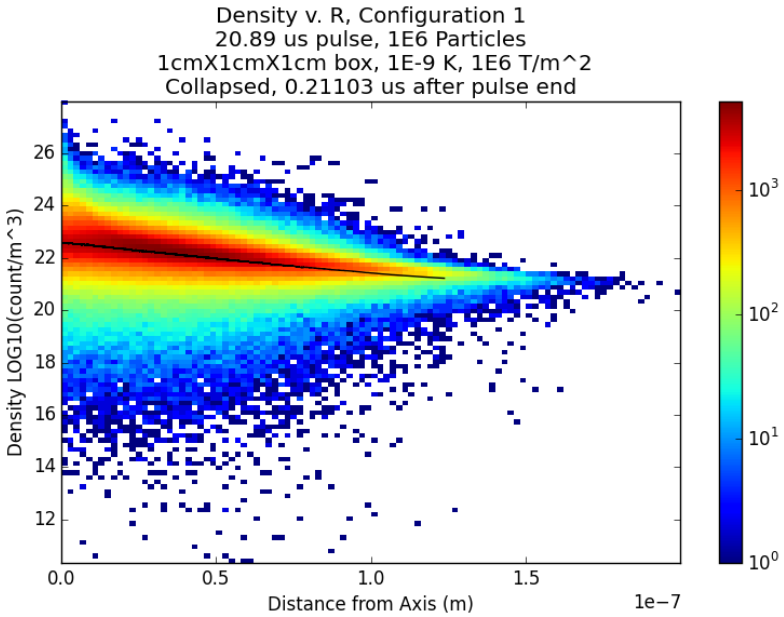

Figure 4: Configuration 1 - Final Density vs. R. The average particle at R is in black. Color indicates number of particles.

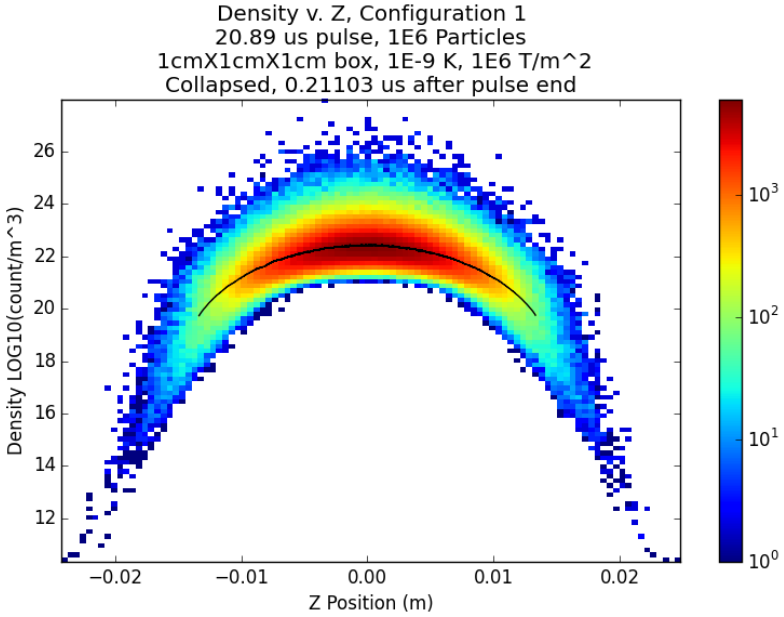

Figure 5: Configuration 1 - Final Density vs. Z. The average particle at Z is in black. Color indicates number of particles.

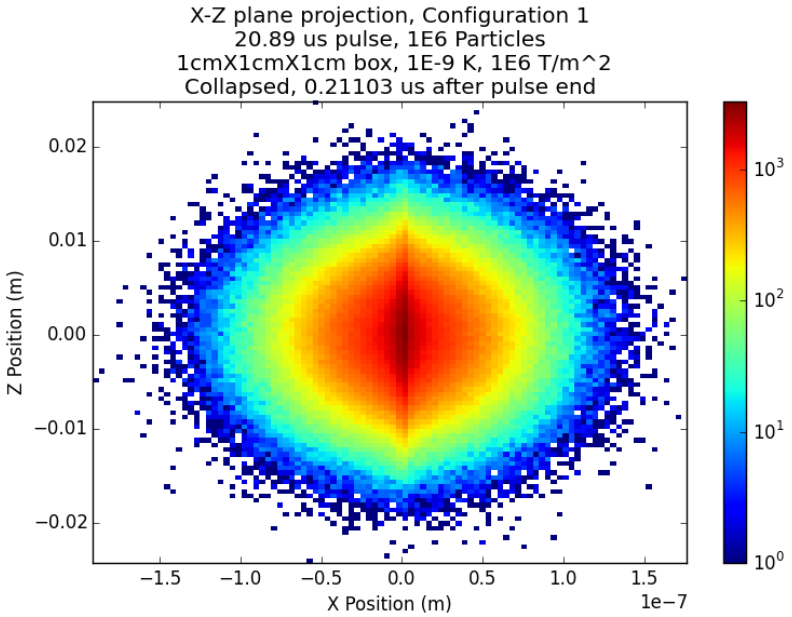

Figure 6: Configuration 1 - Final X-Z projection of particles. Color indicates number of particles.

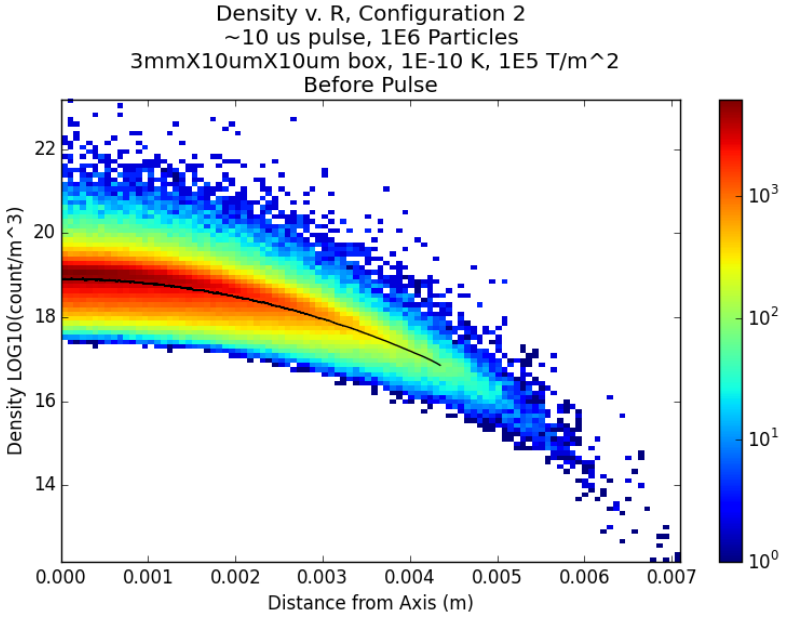

Figure 7: Configuration 2 - Initial Density vs. R. The average particle at R is in black. Color indicates number of particles.

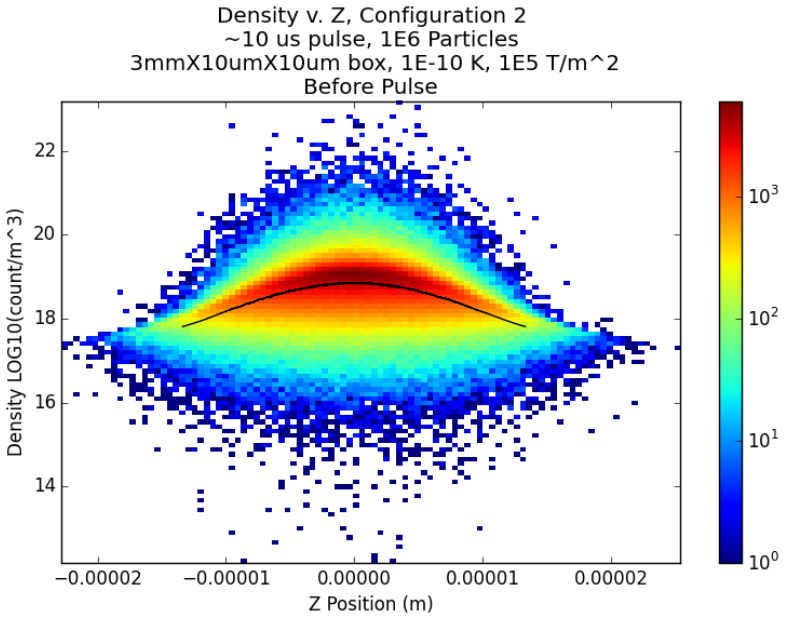

Figure 8: Configuration 2 - Initial Density vs. Z. The average particle at Z is in black. Color indicates number of particles.

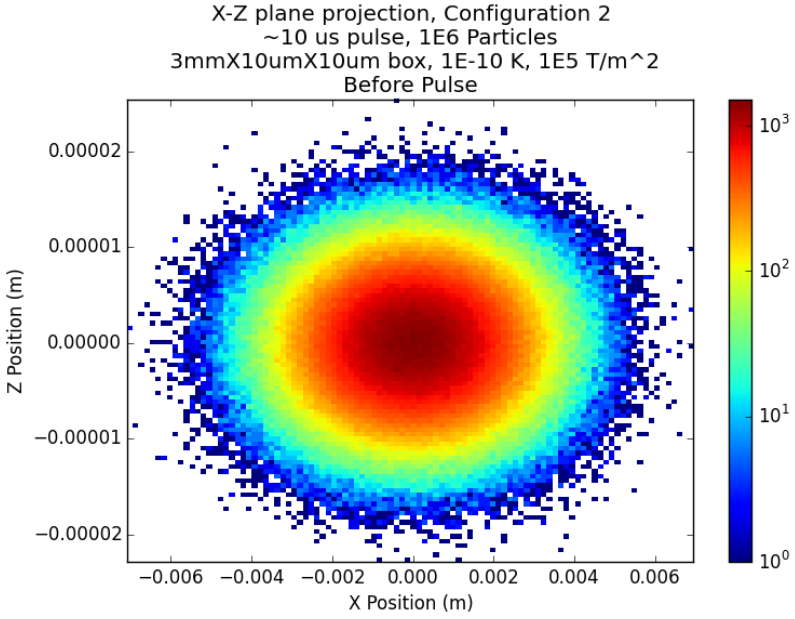

Figure 9: Configuration 2 - Initial X-Z projection of particles. Color indicates number of particles.

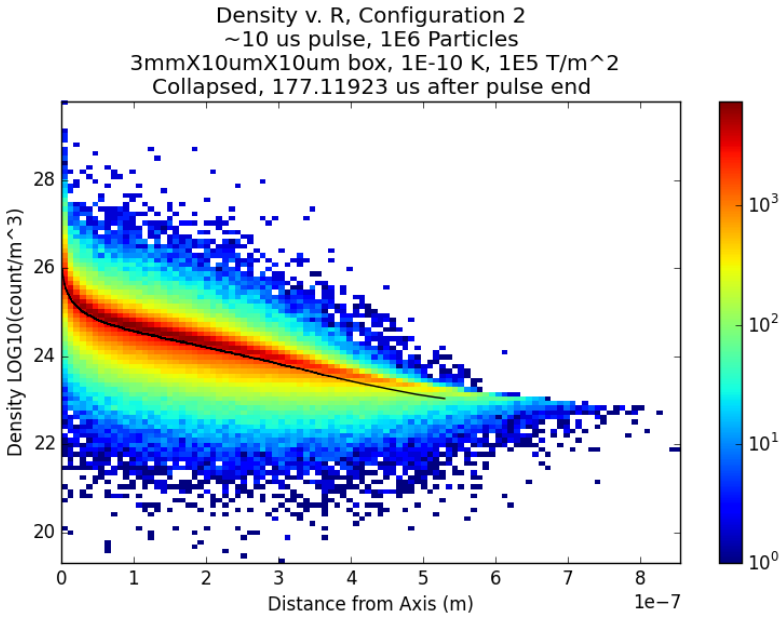

Figure 10: Configuration 2 - Final Density vs. R. The average particle at R is in black. Color indicates number of particles.

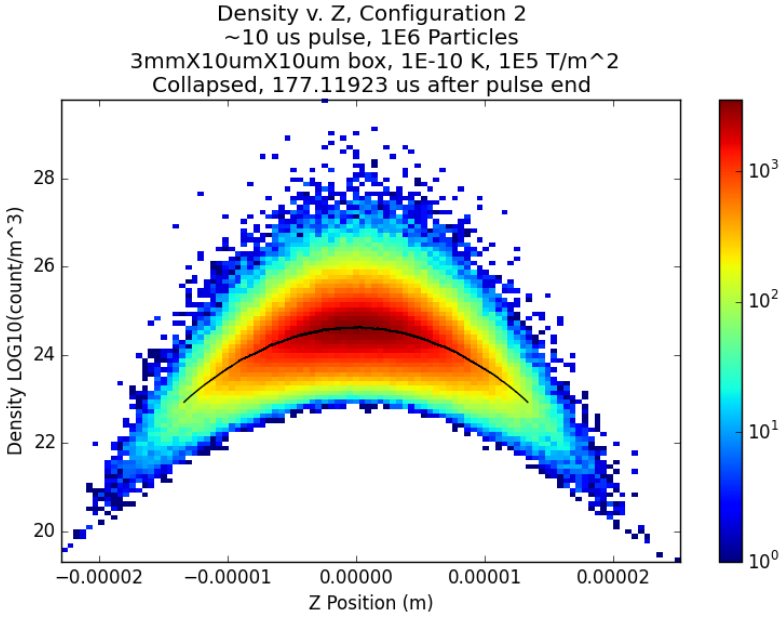

Figure 11: Configuration 2 - Final Density vs. Z. The average particle at Z is in black. Color indicates number of particles.

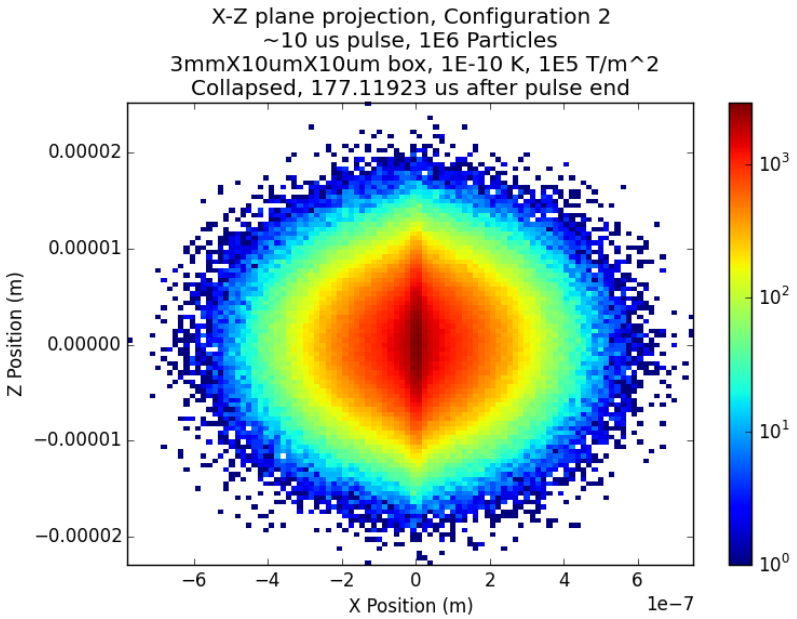

Figure 12: Configuration 2 - Final X-Z projection of particles. Color indicates number of particles.

CHAPTER IV

INTRODUCTION TO IN-SITU SILICON PASSIVATION

The mass of the electron neutrino is an on-going question in the realm of particle physics. Tritium passivated silicon is a proposed alternative to existing sources for β decay electrons [15].

4.1 β Decay for the Mass of the Electron Neutrino

Attempts to measure a bounds on the mass of the electron neutrino typically look at β decay. The reaction that is looked at in general is:

$$ {}^{m}_{n}X \rightarrow {}^{m}_{n+1}Y^{+} + e^{-} + \bar{\nu}_{e}. \tag{25} $$

Here, a species X emits an electron and an anti-neutrino as it changes into another species with the same nuclear mass but with one more proton and one fewer neutron. Typically this is done with tritium in gas phase [16]:

$$ {}^{3}_{1}H \rightarrow {}^{3}_{2}He^{+} + e^{-} + \bar{\nu}_{e}. \tag{26} $$

This reaction has several benefits. First of which is the theoretical exhaustion of hydrogen and its isotopes. The energy released by this reaction is very well known. This energy is distributed among the mass of the helium-3, mass of the electron, mass of the anti-neutrino, and the kinetic energy of all three. Accounting for the mass of helium-3 and electron, 18.6 keV remains for the mass of the anti-neutrino and the kinetic energy of all three particles. Therefore, the current method is to collect the spectrum of the energies of the emitted electron. This spectrum will have a limit before 18.6 keV corresponding to the mass of the electron anti-neutrino. The mass of the electron neutrino is thought to be on the order of single eVs, so there is at

least the requirement of 4 orders of magnitude of precision in any combination of experimental and measurement apparatus [16]. Not only is there this experimental constraint but the fraction of counts in this regime is nearly 10^{-12}. This means that the flux produced in such experiments need to be quite high to build up statistical significance. In experiments with tritium in the gas phase there is a limit on the flux because higher concentrations of tritium gas, while increasing the flux, will also increase scattering events of the electrons off of the tritium gas and resultant helium-3 [17]. These scattering events limit the precision of measurement of the energy spectrum of the electrons.

4.2 Passivated Silicon

Silicon typically forms a crystal in the same structure as a diamond. This crystal structure leaves surface silicon atoms with unbonded electrons, typically called dangling bonds. A filled bond is at a lower energy state than a dangling bond, therefore most molecules and atoms will attempt to fill the bond and attach to the surface.

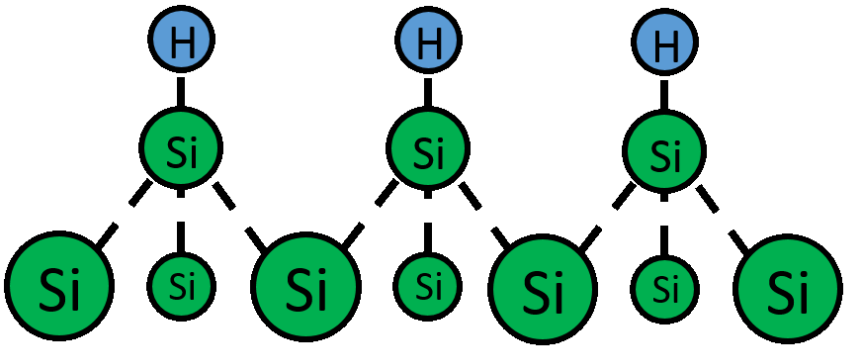

Figure 13: Cross-sectional view of the surface of a hydrogen passivated silicon crystal. The crystal will continue to form the bulk. Only the first two layers of silicon are shown for simplicity.

A certain type of passivation is particularly interesting: hydrogen passivated silicon. In this variety, hydrogen atoms bond to the surface of the silicon. This happens

naturally when the crystal is in an atmosphere of hydrogen atoms. Due to how reactive mono-atomic hydrogen is, when silicon is passivated with hydrogen, it is usually done in a wet chemical environment, but the passivation is quickly depleted by the abundance of oxygen and other chemicals in the atmosphere. Therefore, if this is done in vacuum, a much longer lifetime of the hydrogen passivation can be observed. This is also an ideal environment if one wishes to make β decay measurements.

4.3 Passivated Silicon for a β Decay Source

A tritium (^3_1H) passivated sample of silicon then could be used as an alternative source for β decay electrons [15]. One of the specific advantages for passivated silicon is the limiting of scattering events. The specific reaction that will be used in passivated silicon is:

$$Si_x\left(^3_1H\right) \rightarrow Si_x \multimap +^3_2He^+ + e^- + \bar{\nu}_e \tag{27}$$

Here Si_x is simply the bulk crystal of silicon and $\multimap$ is a dangling bond left by the removal of the hydrogen atom. By affixing all of the tritium to the surface of the silicon there will be limited scattering of the electrons emitted out from the face of the crystal. Flux is therefore limited only by the size of the crystal. For a silicon <111> lattice cleave the surface density of hydrogen is:

$$\sigma_H = \frac{4}{a^2} \tag{28}$$

where a is the lattice constant of the crystal. For Si<111>, $a = 5.431\mathring{A}$. This leads to $\sigma_H = 1.36 \times 10^{19}$ atoms/m^2 [9]. In order to have more counts in the relevant regime of the energy spectrum of the β decay electrons, one simply needs to increase the amount of crystal being used. It is also possible that the chemical bond may influence the β decay energy spectrum. However, the work to predict this is still being performed.

CHAPTER V

METHODS AND MATERIALS OF IN-SITU SILICON PASSIVATION

The following is an overview of the methods that are being used to do in-situ hydrogen passivation of silicon.

5.1 The Choice of Silicon Crystal

The diamond-like crystal of silicon has many manufacturing specifications relevant for ideal hydrogen passivation, such as lattice cleave, dopant, etc. Ones that aid the passivation of the surface are geometries and conditions of the surface that promote ease of access of hydrogen atoms. This is essentially the existence of an exposed dangling bond ($-\circ$) for the following reaction to take place:

$$Si_x - \circ + H \rightarrow Si_x H \tag{29}$$

The existence of the dangling bond is mediated by: 1) the electrons in the crystal and 2) the lack of coverage. Section 5.2 will explore 2) in further detail. However, the electrons in the crystal can be mediated by the doping of the crystal during manufacturing. An N-type doping will promote the abundance of electrons in the crystal to be available for surface dangling bonds.

A <111> lattice cleave allows for the most access to the dangling bonds. This is because the dangling bonds in this lattice cleave are normal to the surface. The enhanced access is apparent when comparing the sticking coefficients to the <100> cleave [18]. Thus, a N-type doped Si<111> wafer is ideal for creating an entirely passivated surface of silicon. The specific crystal used by this experiment is a single-sided polished, Phosphorus doped Si<111> with a 0.1 degree angle miscut wafer that

is 8.0 ± 1.65mm thick and 25.4 ± 0.3 mm in diameter from Virginia Semiconductor Inc.

5.2 Cleaning the Silicon Crystal

5.2.1 RCA Cleaning

To remove organic contaminants from the surface, RCA-I cleaning procedure was used [19]. This leaves a thin oxide layer on the crystal surface that is later removed in the vacuum.

5.2.2 Thermal Desorption

The oxide layer must be removed in vacuum following the RCA-I cleaning and prior to hydrogen passivation. The rate (R_d) of thermal desorption of the oxide layer will follow the Polanyi-Wigner equation [20]:

$$R_d = -\frac{d\theta}{dt} = k_m^0 \theta^m e^{-E_d/k_B T} \tag{30}$$

where θ is the fractional coverage of the surface, E_d is the energy of desorption, k_m^0 is the first order prefactor of the reaction, and T is the temperature of the crystal. The value of E_d for desorption of the oxide layer is 4 eV [21] and the first order prefactor (k_m^0) is 6×10^{13} s^{-1} [20]. This gives a characteristic decay time of the oxide layer at 1200K of:

$$\tau = \frac{1}{k_m^0} e^{E_d/k_B T} \approx 17.5 \text{ minutes} \tag{31}$$

Once this layer is depleted the typical contaminant will take much longer to adhere to the surface at a pressure on the order of 10^{-5} torr. This layer will also be depleted faster by reaction with a hydrogen environment.

In order to heat the silicon crystal to this temperature, a tungsten filament is used. This filament is sandwiched between two thermally conductive but electrically insulating discs made of shapal with a piece of molybdenum acting as the sync to the crystal. The assembled heater can be seen in Figure 14. The silicon wafer (not

pictured) is fastened with the three clips to the molybdenum face to warm the crystal and can be held at elevated temperatures for several times the characteristic time of desorption. With all of this preparation of the crystal in tow, the crystal can then be passivated by hydrogen atoms with few contaminants.

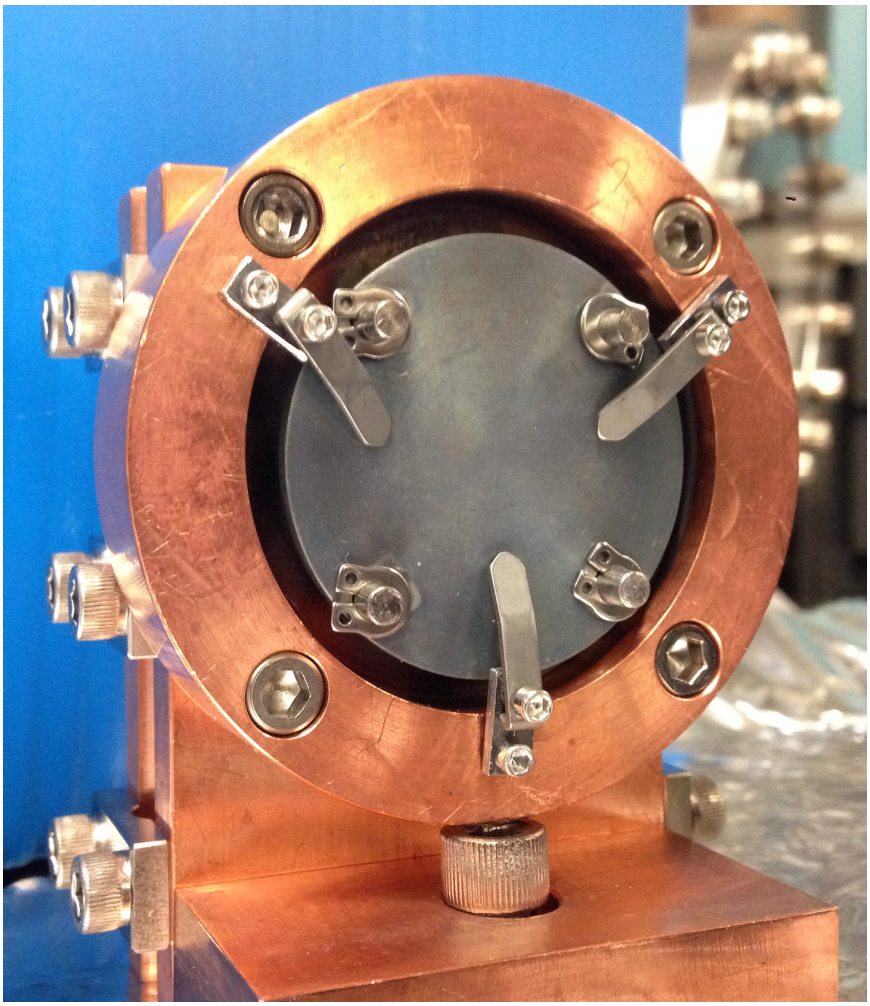

Figure 14: Silicon heater assembly. Shapal discs and tungsten filament are not visible, because they are under the molybdenum face.

5.3 Application of Atomic Hydrogen

5.3.1 Hydrogen Surface Reactions

There are many reactions to consider when looking at the total passivation of the surface. In order to prove the method works for hydrogen isotopes, deuterium (D)

was used. Tritium has several safety constraints that make it unfavorable to work with, mostly due to its half-life of 12 years. Deuterium also provides the added benefit of being detectable over the background hydrogen in the chamber by a Residual Gas Analyzer (RGA). Relevant reactions to passivating the surface of the Si<111> include:

$$D_2 + Si_x \multimap\!\!\rightarrow Si_xD + D \tag{32}$$

$$D + Si_x \multimap\!\!\rightarrow Si_xD \tag{33}$$

$$Si_xD + D \rightarrow Si_x \multimap + D_2. \tag{34}$$

The contributions of these reactions to the passivated layer are best encapsulated in the sticking coefficient of these reactions. The sticking coefficient is simply a likelihood that an incident atom adheres to the surface, as opposed to one coming off. Equation 32 and Equation 34 combine to give a sticking coefficient near 10^{-6} [22]. This is quite small when compared to the sticking coefficients (s) from Equations 33 and 34, which for the uncovered surface is 0.6 [18]. Therefore the molecule disassociating on its own will be neglected.

Taking into account for the percent coverage of the surface (θ) the stick coefficient becomes [22]

$$s = (1-\theta)^2 s_0. \tag{35}$$

Then to find change in coverage the number of incident atoms on the surface per unit surface area (n_I) and the initial density of sites (σ_0) needs to be addressed:

$$\frac{d\theta}{dt} = s\frac{n_I}{\sigma_0} = (1-\theta)^2 s_0 \frac{n_I}{\sigma_0}. \tag{36}$$

This yields a solution for $t > 0$ of:

$$\theta = 1 - \frac{\sigma_0}{s_0 n_I t + \sigma_0}. \tag{37}$$

The number incident on the surface can be arrived at through the ideal gas laws:

$$n_I = \frac{P}{\sqrt{2\pi m k_b T}} \tag{38}$$

for a gas at pressure P, particle mass m, and temperature T.

5.3.2 Atomic Hydrogen Source

As discussed in the previous subsection, the optimal reaction for the general process is one comprised of hydrogen atoms. To achieve this, diatomic hydrogen gas must be split into atoms. Thermal breakdown of the bond is achievable through use of hot tungsten [9]. Hydrogen molecules that come in contact with the filament pick up enough energy to overcome the bonded potential. Specifically for deuterium, but for hydrogen isotopes in general:

$$H_2 + W \rightarrow H + H + W \tag{39}$$

The particular apparatus is shown in Figure 15. The tungsten filament is heated resistively. Pyrometry measurements indicate that the filament achieves 2350 ^{o}C at 310 Watts of power. This is sufficient to thermally excite the bond of the hydrogen molecules to create mono-atomic hydrogen.

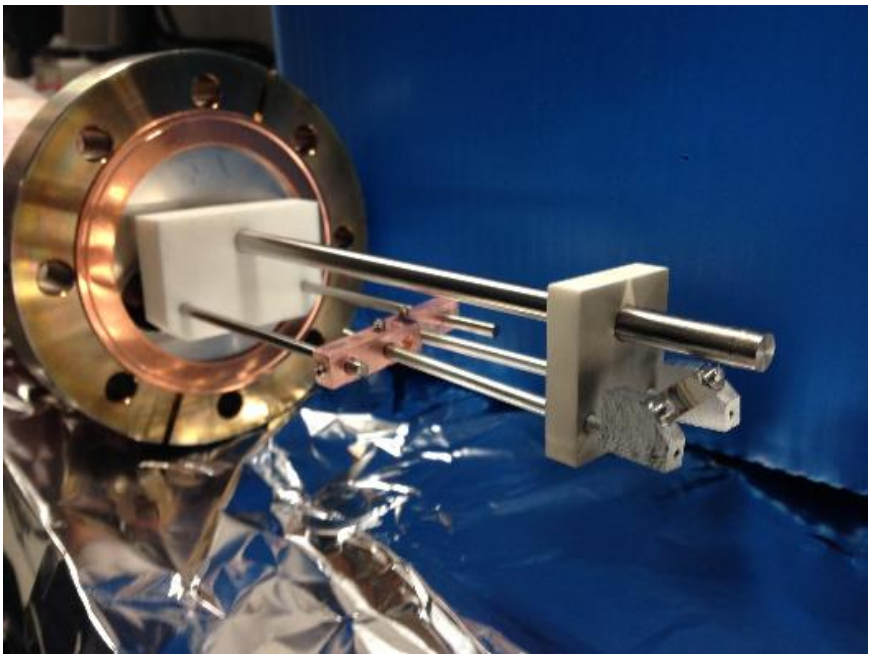

Figure 15: Hot filament hydrogen cracker

This effect has been measured to ensure the effectiveness of the technique. When

any hydrogen isotope collides with the filament it has a high probability to undergo the reaction in Equation 39. Because hydrogen gas will always effuse through the vacuum chamber walls there is always a molecular hydrogen background inside of the chamber at the natural abundances. This means that while the cracker is running, it is actively splitting both background hydrogen and the hydrogen that is being flowed over the filament controlled by a leak valve. Due to the isotopic abundance of deuterium it is safe to assume the majority of deuterium in the chamber is flowed across the filament from the hot filament cracker. When the hydrogen isotopes hit the wall of the chamber they cool and recombine. The reaction that indicates that deuterium is being cracked is:

$$H + D \rightarrow HD. \tag{40}$$

HD can be sensed by a Residual Gas Analyzer (RGA) with relative ease. HD is the only way a 3 amu signal can be seen in the RGA in our vacuum system as ^{3}He is not present. This has been observed and can be seen in the output of the RGA in Figures 16 and 17 where the filament is at 1835 ^{o}C. Notice the 3 amu peak (HD) in between the 2 amu peak(H_2 and D) and 4 amu (D_2) in Figure 17. Therefore, this will effectively dose the surface of the silicon at a pressure near 10^{-7} torr as measured by the RGA and tuned by leak valve.

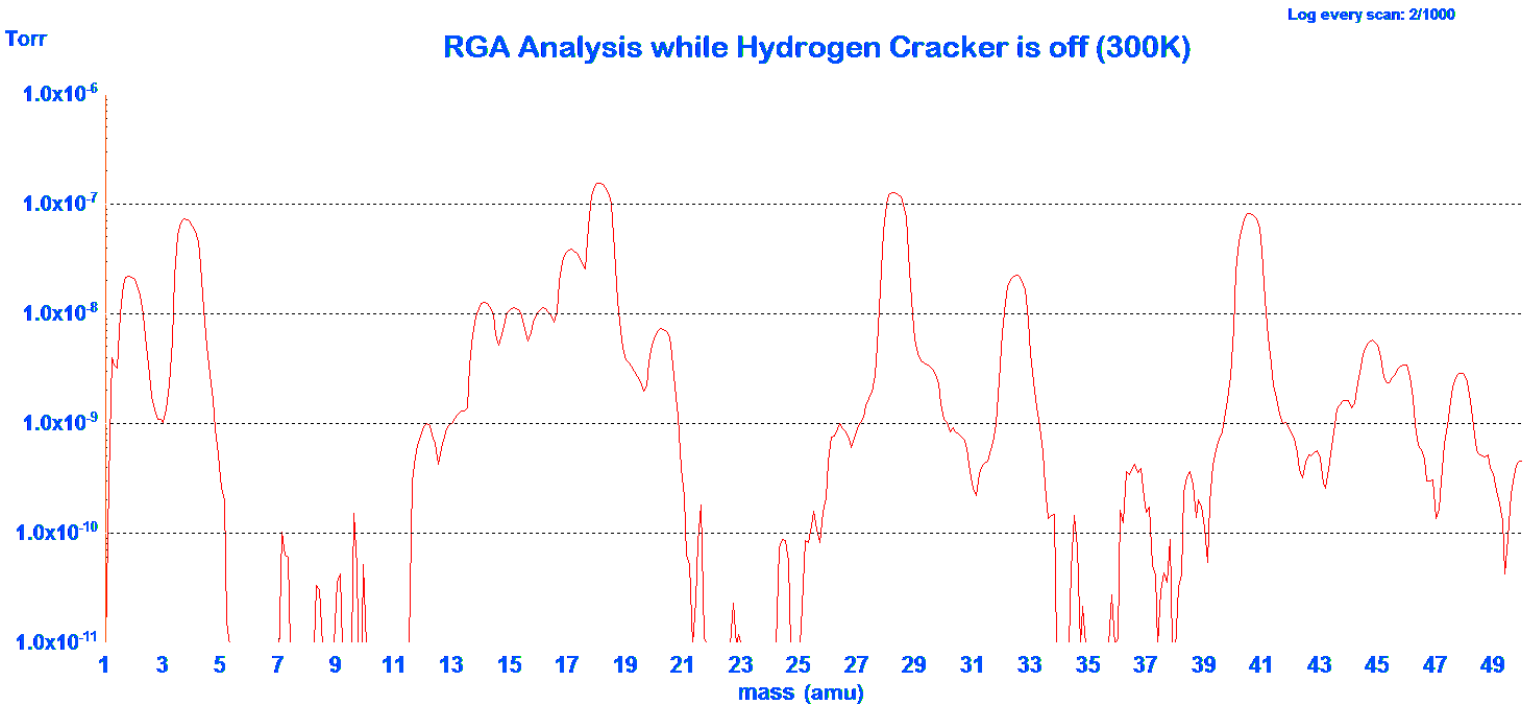

Figure 16: RGA spectrum prior to heating of the filament.

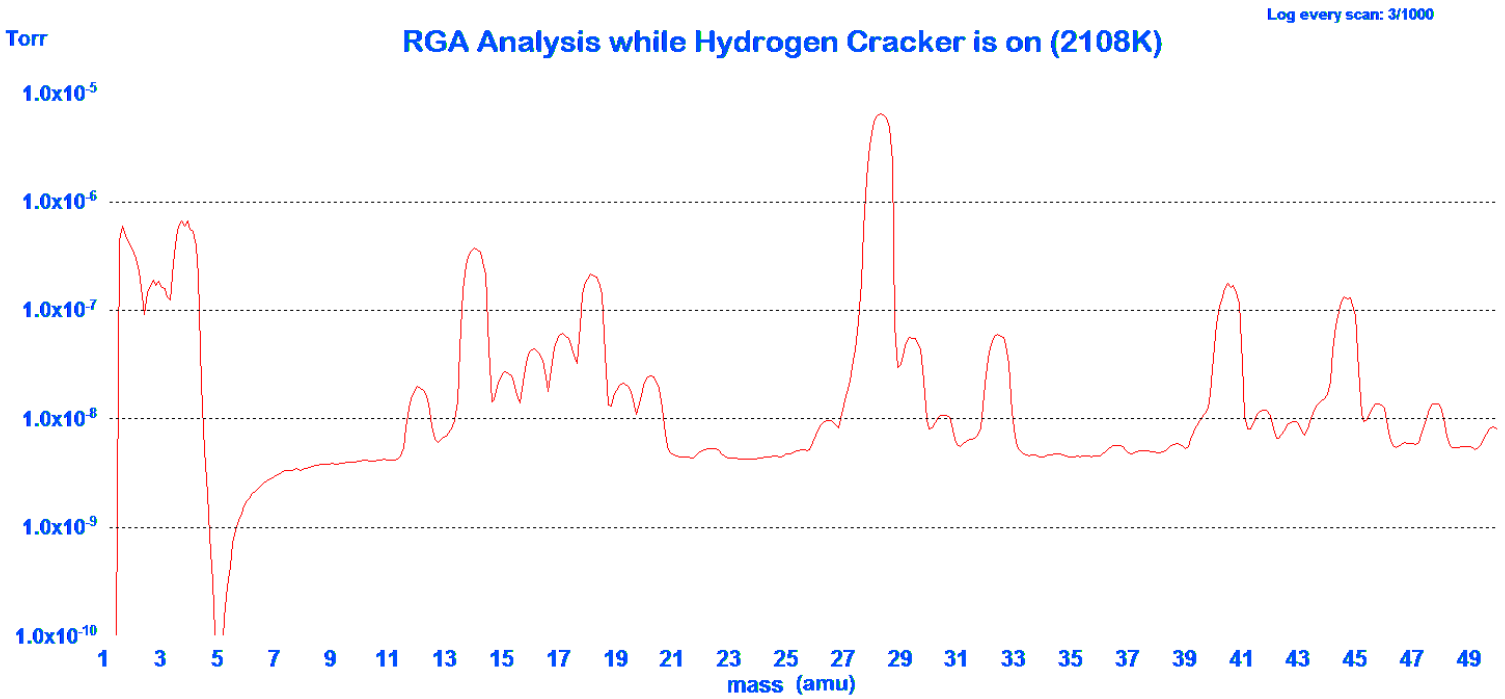

Figure 17: RGA spectrum while filament is on.

CHAPTER VI

RESULTS OF IN-SITU SILICON PASSIVATION

Measurements of the passivated silicon crystal have yet to be carried out due to complications with the vacuum chamber pressure. However, outlined below are the methods for determining the quality of the layer while in vacuum.

6.1 Debye-Waller Factor

A simple way to address the surface passivation without relocation of the wafer to an electron microscope is specular reflection of atoms off of the surface. Given the initial confirmation that passivation is occurring through specular reflection off of the surface, further characterization would be ideal.

The specular reflection intensity (I) of an incident source of atoms with intensity I_0 is given by the Debye-Waller Factor[23]:

$$\frac{I}{I_0} = e^{-2W}. \tag{41}$$

W is defined as:

$$W = \frac{12m(E_\perp + D)T}{Mk_b\theta_D^2} \tag{42}$$

where m is the mass of the incident atoms, $E_\perp$ is the Energy perpendicular to surface, D is the well depth of the interaction, T is the temperature of the crystal, M is the mass of a surface atom, and θ_D is the Debye temperature of the crystal. In the system used, the well depth (D) is negligible when compared to the energy incident to the surface ($E_\perp$). While the surface of the silicon is passivated with hydrogen, the Debye-Waller factor is phonon dependent and is dominated by the silicon lattice structure and not the hydrogen [24]. The hydrogen atoms pick up the lattice structure

delegated to them by the silicon crystal. Thus, M is the mass of a silicon atom and θ_D is the Debye temperature of the silicon crystal.

The Debye-Waller factor is limited to clean crystals and well-passivated surfaces because of the phonon dependence. Crystals with surface defects will have disorganized phonon modes excited when incident atoms interact with the surface. Therefore many fewer incident atoms will fall into the elastic scattering channels that the Debye-Waller factor sums over, and much fewer will fall into those observed as specular reflection by a detector.

6.2 Reflection of a Helium Beam

Using the Debye-Waller factor as a springboard, helium can be used as an incident atom beam. This will produce the highest magnitude of reflected intensity as given by the Debye-Waller factor in Section 6.1. Hydrogen molecules cannot be used because the surface interaction will excite rotational states in the molecules that cannot be measured, and hydrogen atoms cannot be used because of the reaction in Equation 34. ^{3}He would produce slightly higher intensities but is not economically sound for this application. At room temperature, helium from a supersonic nozzle will travel at 1870 m/s [24]. Thus a peak reflection amplitude at 45^o off of a 500K crystal should be 11.7%. The remaining 88.3% is lost to the vacuum via inelastic scattering off of the crystal.

6.2.1 Helium Supersonic Nozzle

In order to have a uniform beam of incident helium atoms, a supersonic nozzle must be used [24]. The supersonic beam has a much smaller velocity spread in the beam's co-moving frame. The nozzle used is a Series 9 pulse valve from Parker. This nozzle can operate as fast as 160 μs. In order to reduce the divergence of the helium incident on the crystal a skimmer of 5mm opening diameter from Beam Dynamics is placed after the nozzle. The skimmer shaves off fringes of the supersonic pulse that are

moving away from the center of the beam. This results in a beam that is divergent by 0.5^o and allows for better temporal localization of the beam. The reflection can be gauged based on the differential signal of pressure in an RGA.

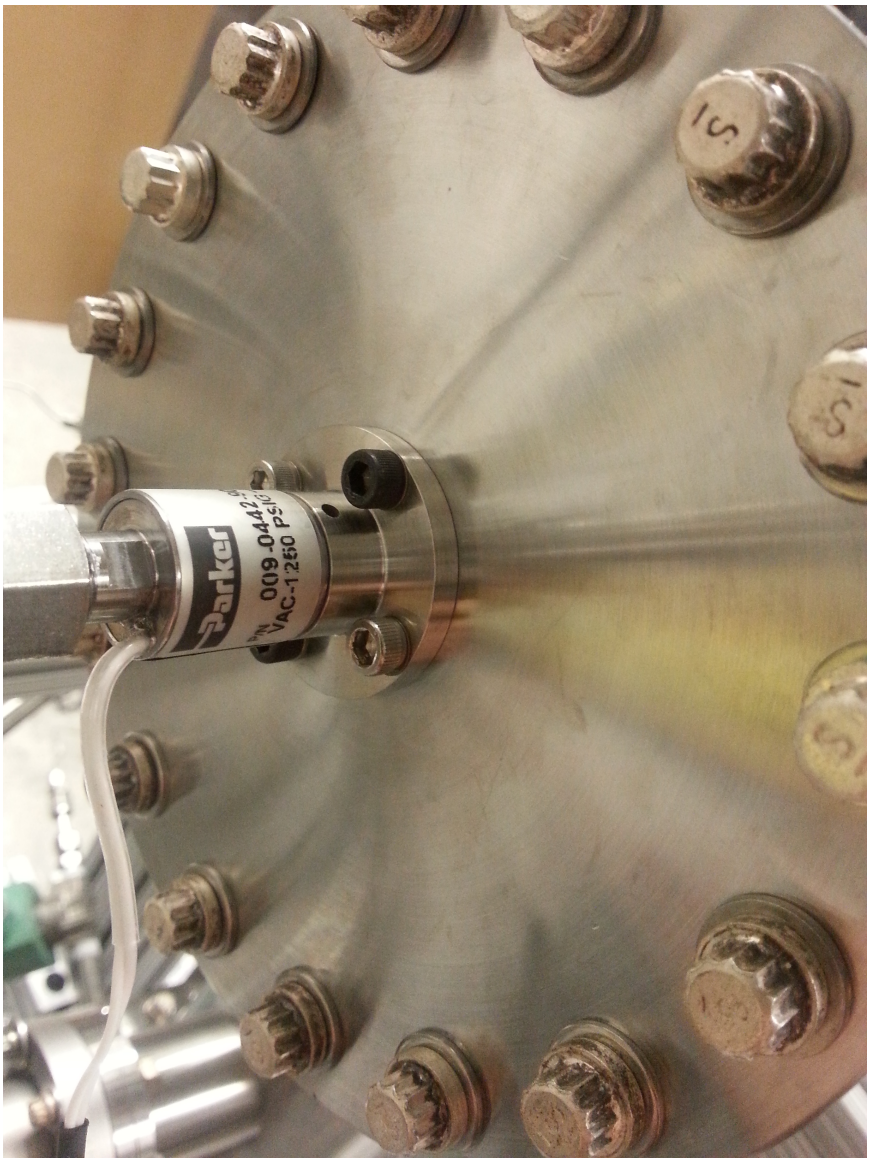

Figure 18: Parker Series 9 pulse valve[25]

6.2.2 Time of Flight Analysis

The supersonic beam is sent into an RGA after being reflected from the crystal. This results in a signal above the background of helium in the vacuum chamber. For

reference, Figure 19 is the signal received by the RGA by passing the beam straight through the chamber. Figure 20 shows a drawing of the chamber and the path of the helium atoms. Figure 21 is the assembled set-up that needs only a few problems solved before this analysis can be done.

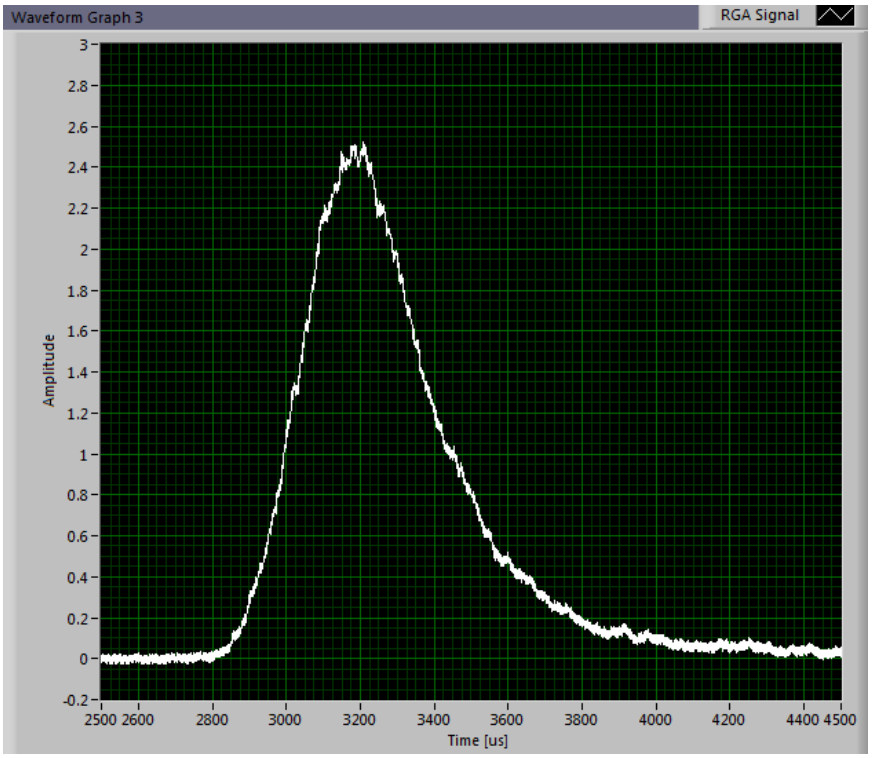

Figure 19: RGA signal of a helium beam from the Parker Series 9 Valve using time of flight techniques when the beam travels through the chamber without interaction.

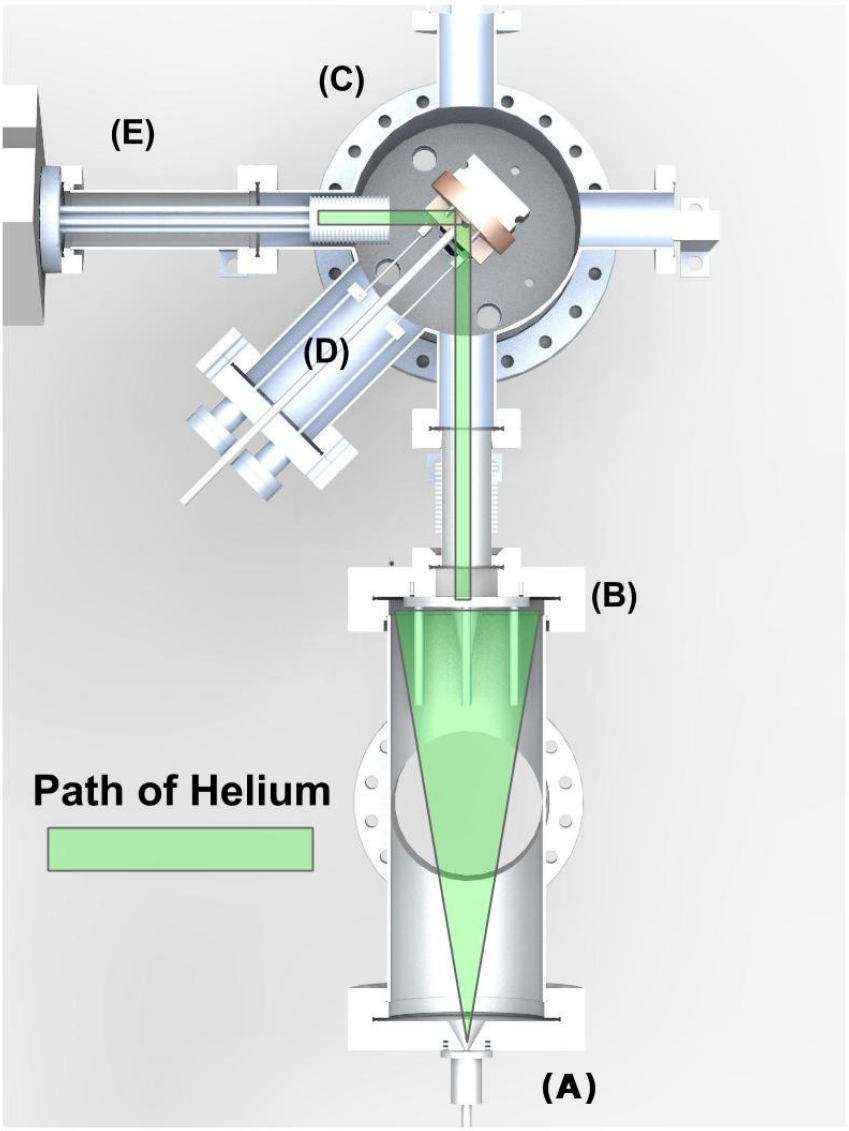

Figure 20: Vacuum chamber with all parts. Path of helium in green. Parts: A)nozzle, B) skimmer, C) silicon heater, D) hot filament cracker, E) RGA.

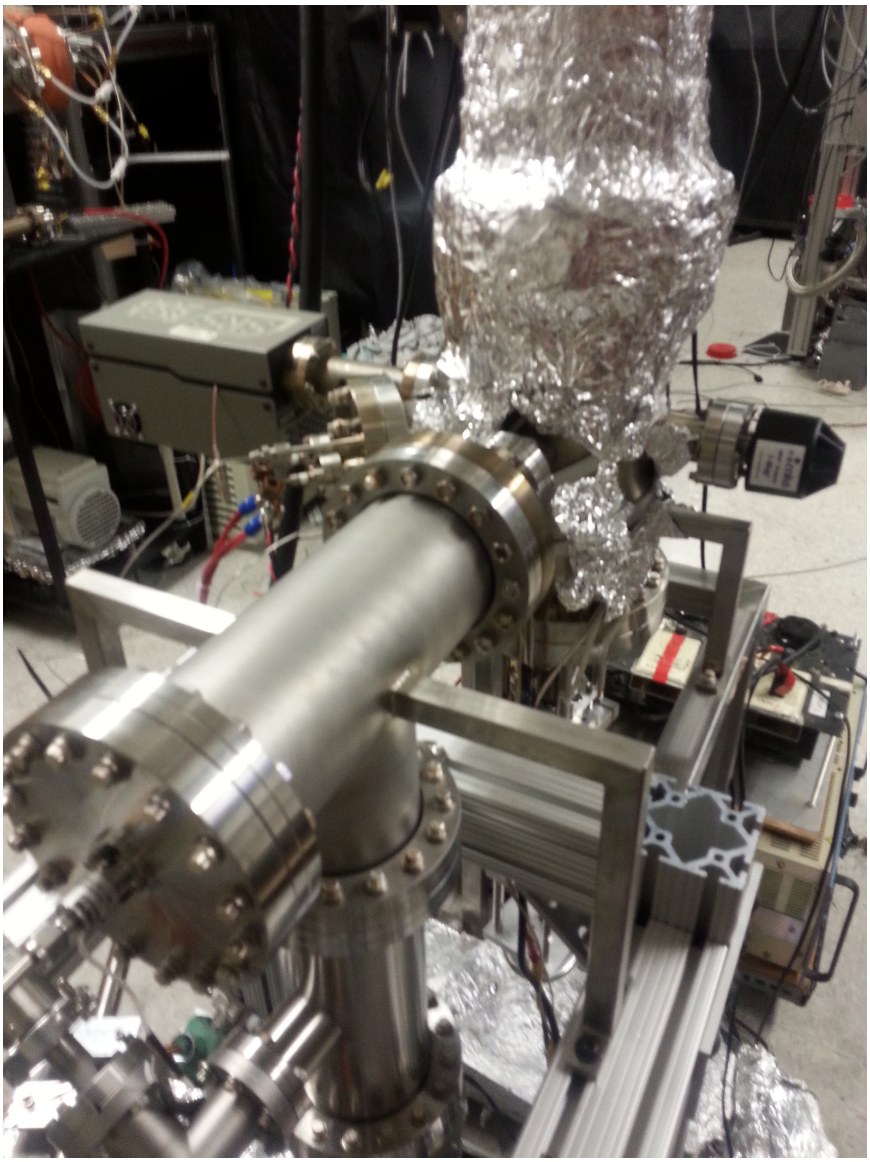

Figure 21: Assembled vacuum chamber.

CHAPTER VII

FUTURE WORK OF IN-SITU SILICON PASSIVATION

Several avenues are left to be traveled by this work, the first of which is actual observation of the passivation layer now that all of the mechanics have been resolved and the apparatus has been assembled. After inital observation, optimization of the passivation layer and procedure can still be achieved, including desorption times, hydrogen dosing, etc. This work outlines many of the constraints and will now proceed to discuss some areas of improvement before tritium passivation can occur.

7.1 Hydrogen Cracker

An improvement to the hot filament hydrogen cracker has already been developed. This model, shown in Figure 22 and 23, uses a hot tungsten capillary heated by thermionic electrons to split the hydrogen in the same process as the hot filament hydrogen cracker. The dimensions of the capillary are such that it is likely that room temperature hydrogen gas will come in contact with the capillary walls before exit. The benefits of this design are increased directional outflow of the hydrogen atoms and protection of the passivation layer from the radiation. It was noticed, due to radiation, that the hot filament cracker may have been depleting the passivation layer as it was applied. Therefore this newer model includes a heat shield to block the majority of the radiation, while still spraying the silicon with atomic hydrogen. This model has not been tested yet due to acquisition of power supplies for the thermionic emission.

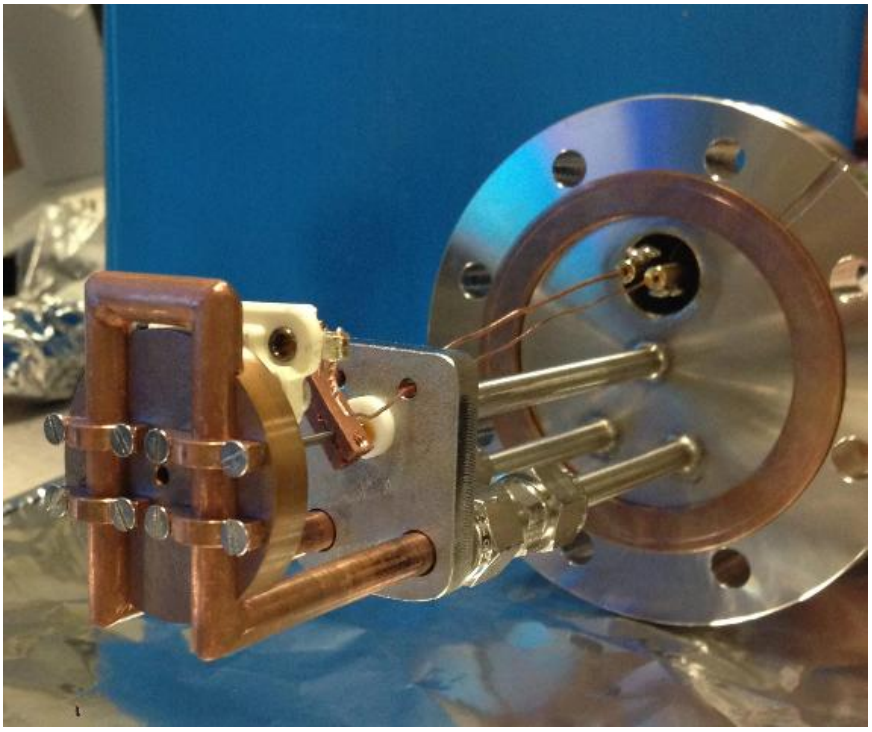

Figure 22: Revised design of hydrogen cracker.

7.2 Silicon Heater

Due to the temperature dependence of the Debye-Waller factor, it would be helpful to cool the silicon after it has been heated for desoprtion. if the passivated crystal could be lowered to room temperature, the reflection could be as much as 27% of the incident beam.

7.3 Chamber

The main advantage to the experiment being in vacuum is the longer lifetime of the passivation layer. The lower pressure will also maintain the integrity of the helium beam for specular reflection. Thus, pressure improvements are doubly helpful.

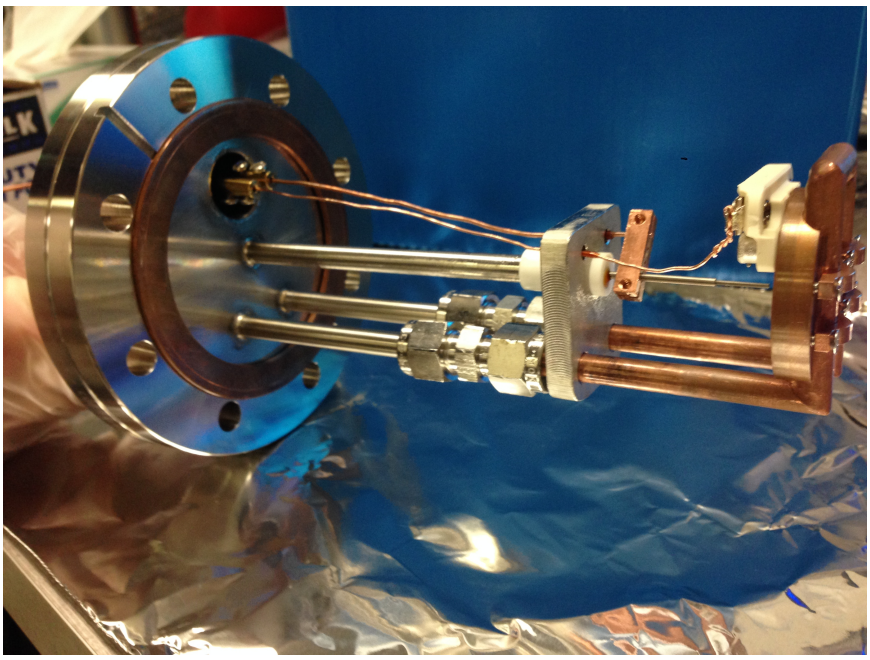

Figure 23: Revised design of hydrogen cracker. View of tungsten capillary.

APPENDIX A

CLOSED FORM DERIVATION OF COLLAPSE TIME OF HYDROGEN CLOUD

In order to more quickly find the peak density, the following derivation was used to find the collapse time of the the hydrogen cloud in the hexapole lens.

A.1 Set-Up

Classically, with no forces acting on a particle, the position of a particle at some time t is:

$$r_f = r_0 + v_r t \tag{43}$$

where v_r is the velocity in the r direction or $\hat{r} \cdot \vec{v}$. Assuming the particle starts at some distance $r_0 = r$ and travels to $r_f = 0$ this is expected to happen in time:

$$t = -\frac{r}{v_r}. \tag{44}$$

The average time for a particle to follow this condition (which will be the time of peak density $t_{collapse}$) is then for n particles:

$$t_{collapse} = \frac{-1}{n} \Sigma_i^n \frac{r}{v_r}. \tag{45}$$

Or more conveniently:

$$t_{collapse} = -\left\langle \frac{r}{v_r} \right\rangle. \tag{46}$$

A.2 Substitution of Relevant Constraints

Based on a harmonic potential of the hexapole lens, the following differential equation is relevant (this equation the same as Equations 11 and 12, the only difference being

that the substitution $r^2 = x^2 + y^2$ has not been made):

$$\frac{d^2r}{dt^2} = -\omega^2 r \tag{47}$$

The solutions of r for this are then:

$$r = r_0 \cos(\omega t_d) + \frac{v_{r,0}}{\omega} \sin(\omega t_d) \tag{48}$$

where t_d is the time that the particles are driven in harmonic potential. This solution can be rewritten as:

$$r = \sqrt{r_0^2 + \frac{v_{r,0}^2}{\omega^2}} \cos(\omega t_d + \phi) \tag{49}$$

where $\phi = \arctan\left(\frac{v_{r,0}}{\omega r_0}\right)$. The derivative of Equation 49 is simply v_r. Substituting back into Equation 46 this removes dependence of the initial state of the cloud except for the ϕ dependence:

$$t_{collapse} = \left\langle \frac{\cos(\omega t_d + \phi)}{\omega \sin(\omega t_d + \phi)} \right\rangle. \tag{50}$$

A few angle addition trigonometric identities will then convert this to:

$$t_{collapse} = \left\langle \frac{\cos(\omega t_d)\cos(\phi) - \sin(\omega t_d)\sin(\phi)}{\omega(\sin(\omega t_d)cos(\phi) + \cos(\omega t_d)\sin(\phi))} \right\rangle. \tag{51}$$

Now a consideration of ϕ must be done. Assuming all r_0 are positive quantities to begin with and that there is no preferential alignment of $v_{r,0}$ with $\hat{r}_0$, the average $\sin(\phi) = 0$ and $\cos(\phi) = \beta$, which is dependent on the initial temperature of the hydrogen in the hexapole lens. This temperature dependent constant cancels out to leave Equation 23:

$$t_{collapse} = \frac{\cot(\omega t_d)}{\omega}. \tag{52}$$

APPENDIX B

SCALING OF FINAL DENSITY APPROXIMATION

To find parameters that are suitable for simulation it is convenient to have the approximate scaling of the final parameters of the cloud as it collapses. The following is a derivation of an approximation of the peak density profile of the cloud.

Equation 48 gives the initial position of the particle once it reaches the collapse phase of the particles in the hexapole lens. Once the lens is turned off, the equations of motion in the Cartesian system are of the form:

$$r_{i,f} = r_{i,post-drive} + t_{collapse} v_{i,post-drive} \tag{53}$$

$$r_{i,post-drive} = r_{i,0}\cos(\omega t_d) + \frac{v_{i,0}}{\omega}\sin(\omega t_d) \tag{54}$$

$$v_{i,post-drive} = -r_{i,0}\omega\sin(\omega t_d) + v_{i,0}\cos(\omega t_d) \tag{55}$$

$$z_f = z_0 + v_{z,0}(t_d + t_{collapse}) \tag{56}$$

where the i subscript can be replaced with either x or y, the $post-drive$ subscript denotes positions and velocities immediately after the harmonic potential is turned off, the 0 subscript denotes the initial conditions of the particles before the harmonic drive, and f denotes that this is at some time later (the final time). Because the simulation starts with a Gaussian distribution, it is a reasonable approximation to model the final form of the distribution. That is:

$$\rho = n\left(\frac{1}{\sqrt{2\pi}}\right)^3 \frac{1}{\sigma_x\sigma_y\sigma_z} e^{-\frac{x^2}{2\sigma_x^2}-\frac{y^2}{2\sigma_y^2}-\frac{z^2}{2\sigma_z^2}}. \tag{57}$$

And σ_i is the standard deviation of the distribution given by:

$$\sigma_i = \sqrt{\langle r_i^2\rangle - \langle r_i\rangle^2}. \tag{58}$$

Therefore, it is necessary to find the values of $\langle x_f \rangle$, $\langle x_f^2 \rangle$, $\langle y_f \rangle$, $\langle y_f^2 \rangle$, $\langle z_f \rangle$, and $\langle z_f^2 \rangle$. These can be found from Equations 53, 54, 55, and 56. From this, we see that both x and y follow the same forms:

$$r_{i,f} = r_{i,0}\cos(\omega t_d) + \frac{v_{i,0}}{\omega}\sin(\omega t_d) + t_{collapse}(-r_{i,0}\omega\sin(\omega t_d) + v_{i,0}\cos(\omega.t_d)) \tag{59}$$

Substituting in the conclusion from Appendix A in Equation 52:

$$r_{i,f} = r_{i,0}\cos(\omega t_d) + \frac{v_{i,0}}{\omega}\sin(\omega t_d) + \frac{\cot(\omega t_d)}{\omega}\left(-r_{i,0}\omega\sin(\omega t_d) + v_{i,0}\cos(\omega t_d)\right) \tag{60}$$

which simplifies to:

$$r_{i,f} = \frac{v_{i,0}}{\omega\sin(\omega t_d)}. \tag{61}$$

Therefore, $\langle x_f \rangle$, $\langle x_f^2 \rangle$, $\langle y_f \rangle$, and $\langle y_f^2 \rangle$ go as:

$$\langle r_{i,f} \rangle = \frac{\langle v_{i,0} \rangle}{\omega\sin(\omega t_d)} = 0 \tag{62}$$

$$\langle r_{i,f}^2 \rangle = \frac{\langle v_{i,0}^2 \rangle}{\omega^2\sin^2(\omega t_d)}. \tag{63}$$

$\langle z \rangle$ and $\langle z^2 \rangle$ are much simpler to derive because there are never any forces in the z direction, yielding:

$$\langle z_f \rangle = \langle z_0 \rangle + \langle v_{z,0} \rangle \left(t_d + \frac{\cot(\omega t_d)}{\omega}\right) = 0 \tag{64}$$

$$\langle z_f^2 \rangle = \langle z_0^2 \rangle + \langle v_{z,0}^2 \rangle \left(t_d + \frac{\cot(\omega t_d)}{\omega}\right)^2. \tag{65}$$

Lastly, the relation of temperature to these velocities must be used to make the entire solution dependent on the initial starting temperature:

$$\langle v_{i,0}^2 \rangle = \frac{k_b T_0}{m}. \tag{66}$$

Substituting all of this information back into Equation 57 yields the approximation for the resultant peak density as a function of space:

$$\rho = n\left(\frac{1}{\sqrt{2\pi}}\right)^3 \frac{m\omega^2\sin^2(\omega t_d)}{k_b T_0\sqrt{\frac{L_z^2}{4} + (t_d + \cot(\omega t_d))^2\frac{k_b T_0}{m}}} e^{-\frac{m\omega^2\sin^2(\omega t_d)(x^2+y^2)}{2k_b T_0} - \frac{z^2}{2(L_z^2/4 + (t_d+\cot(\omega t_d))^2 k_b T_0/m)}} \tag{67}$$

APPENDIX C

SCALING OF FINAL TEMPERATURE APPROXIMATION

To find parameters that are suitable for simulation it is convenient to have the approximate scaling of the final parameters of the cloud as it collapses. The following is a derivation of an approximation of the final temperature of the cloud.

The basic forms of temperature (T) and energy (E) relations from thermodynamics are:

$$T = \frac{2}{3k_b}\langle E\rangle = \frac{m}{3k_b}(\langle v_x^2\rangle + \langle v_y^2\rangle + \langle v_z^2\rangle) \tag{68}$$

$$\langle v_i^2\rangle = \frac{k_b T}{m} \tag{69}$$

where k_b is the Boltzmann constant, m is the mass of the particle, and v_i is the velocity in the i direction in Cartesian coordinates. The velocity of the particles will not change after the drive so $v_{i,f} = v_{i,post-drive}$ which is Equation 55 for x and y directions. The $r_i v_i$ cross term is again 0 so that:

$$\langle v_{i,f}^2\rangle = \langle r_{i,0}^2\rangle \omega^2 \sin^2(\omega t_d) + \langle v_{i,0}^2\rangle \cos^2(\omega t_d) = \frac{L_i^2}{4}\omega^2 \sin^2(\omega t_d) + \frac{k_b T_0}{m}\cos^2(\omega t_d) \tag{70}$$

where the z direction velocities are unchanged. This leads to:

$$\langle v_{z,f}^2\rangle = \langle v_{z,0}^2\rangle = \frac{k_b T_0}{m}. \tag{71}$$

Therefore, the final temperature is:

$$T_f = \frac{m}{3k_b}\left(\frac{k_b T_i}{m}(1 + 2\cos^2(\omega t_d)) + \frac{L_x^2 + L_y^2}{4}\omega^2 \sin^2(\omega t_d)\right). \tag{72}$$

REFERENCES

[1] R. J. Gould, *The Interstellar Abundance of the Hydrogen Molecule*, Cornell University (1963).

[2] M. J. Turk *et al.*, *Effects of Varying the Three-Body Molecular Hydrogen Formation Rate in Primordial Star Formation*, SLAC-PUB-14304 (2010).

[3] M. J. Turk, T. Abel, and B. O'Shea, *The Formation of Population III Binaries from Cosmological Initial Conditions*, Science (2009).

[4] H. Kreckel *et al.*, *Experimental Results for H_2 Formation from H and H and Implications for First Star Fomration*, Science (2010).

[5] D. R. Flower and G. J. Harris, *Three-body recombination of hydrogen during primordial star formation*, Monthly Notices of the Royal Astronomical Society **377**, 705 (2007).

[6] R. C. Forrey, *Rate of Formation of Hydrogen Molecules by Three-body Recombination during Primordial Star Formation*, The Astrophysical Journal Letters **773**, L25 (2013).

[7] D. A. Bell *et al.*, *Relaxation and recombination in spin-polarized atomic hydrogen*, Phys. Rev. B **34**, 7670 (1986).

[8] T. A. Jacobs, R. R. Giedt, and N. Cohen, *Kinetics of Hydrogen Halides in Shock Waves. II. A New Measurement of the Hydrogen Dissociation Rate*, The Journal of Chemical Physics **47**, 54 (1967).

[9] D. Raimi-Zlatic, *Storing and Focusing Atomic Hydrogen to Measure the Rate of Reaction of Three Body Association*, University of Texas at Austin Undergraduate Thesis (2014).

[10] D. W. Savin, *Laboratory measurements of primordial chemistry*, AIP Conf. Proc. (2012).

[11] R. Castillo-Garza, J. Gardner, S. Zisman, and M. G. Raizen, *Nanoscale Imaging of Neutral Atoms with a Pulsed Magnetic Lens*, ACS Nano **7**, 4378 (2013), PMID: 23544794.

[12] *Atomic Physics* (Oxford University Press, 2005).

[13] N. Mohamed, *Efficient Algorithm for Generating Maxwell Random Variables*, Journal of Statistical Physics **145**, 1653 (2011).

[14] P. Tarazona, J. Cuesta, and Y. Martinez-Raton, *Density Functional Theories of Hard Particle Systems*, in *Theory and Simulation of Hard-Sphere Fluids and Related Systems*, edited by A. Mulero, , Lecture Notes in Physics Vol. 753, pp. 247–341, Springer Berlin Heidelberg, 2008.

[15] A. Libson, M. Jerkins, and M. Raizen, *An investigation of tritium passivated silicon as a source for beta-decay experiments*, in *APS Texas Sections Spring Meeting Abstracts*, p. C5004, 2010.

[16] G. Drexlin, V. Hannen, S. Mertens, and C. Weinheimer, *Current Direct Neutrino Mass Experiments*, Advances in High Energy Physics (2013).

[17] M. Jerkins, J. R. Klein, J. H. Majors, F. Robicheaux, and M. G. Raizen, *Using cold atoms to measure neutrino mass*, New Journal of Physics **12**, 043022 (2010).

[18] U. Hansen and P. Vogl, *Hydrogen passivation of silicon surfaces: A classical molecular-dynamics study*, Phys. Rev. B **57**, 13295 (1998).

[19] Virginia Semiconductor*, Wet-Chemical Etching and Cleaning of Silicon.*

[20] G. A. Reider, U. Hofer, and T. F. Heinz, *Desorption kinetics of hydrogen from the Si(111)77 surface*, The Journal of Chemical Physics **94**, 4080 (1991).

[21] Y. Enta, H. Nakazawa, S. Sato, H. Kato, and Y. Sakisaka, *Silicon thermal oxidation and its thermal desorption investigated by Si 2p core-level photoemission*, Journal of Physics: Conference Series (2010).

[22] P. Bratu *et al.*, *Reaction dynamics of molecular hydrogen on silicon surfaces*, Phys. Rev. B **54**, 5978 (1996).

[23] D. Farias and K.-H. Rieder, *Atomic beam diffraction from solid surfaces*, Reports on Progress in Physics **61**, 1575 (1998).

[24] A. Libson, *General Methods of Controlling Atomic Motion: Experiments with Supersonic Beams as a Source of Cold Atoms*, PhD thesis, The University of Texas at Austin, 2012.

[25] Parker Pulse Valves*, Pulse Valves- Ultra Low Leak Extreme Performance Valve.*